Patterning via optical-saturable transformations: A review and simple simulation model

Precious Cantu, Trisha L. Andrew, and Rajesh Menon

Patterning via optical-saturable transformations: A review and simple simulation model

Precious Cantu,[1] Trisha L. Andrew,[2] and Rajesh Menon[1,a]

[1]*Department of Electrical and Computer Engineering, University of Utah, Salt Lake City, Utah 84112, USA*
[2]*Department of Chemistry, University of Wisconsin-Madison, Madison, Wisconsin 53706, USA*

Most of the nanoscale fabrication in the semiconductor industry is based on patterning with scanning-electron beam lithography (SEBL). Although this approach is very versatile and has very high resolution, it is intrinsically a serial writing process, and therefore, relatively slow. Our group has been investigating alternative nano-fabrication techniques, adapted from ideas of saturating optical transitions such as those used in stimulated emission-depletion microscopy and related methods, and optical interference lithography. Linewidths and resolutions on the scale of a few tens of nanometers and below are highly desirable for various applications in nanotechnology. However, the spatial resolution of optical lithography is restricted by diffraction. In the past, we developed absorbance modulation to overcome this limit. This approach utilizes photochromic molecules that can be optically switched between two thermally stable states, one opaque and the other transparent. However, absorbance modulation is limited to surface (2-D) patterning. Here, we report on an alternative approach that exploits unique combinations of spectrally selective reversible and irreversible photochemical transitions to achieve deep subwavelength resolution with potential extension to 3-dimensions. This approach, which we refer to as patterning via optical-saturable transformations have the potential for massive parallelism, enabling the creation of nanostructures and devices at a speed far surpassing what is possible with SEBL. The aim of our research is to translate the success in circumventing Abbe's diffraction limit in optical microscopy to optical lithography. © 2014 AIP Publishing LLC. [http://dx.doi.org/10.1063/1.4902024]

Today the role of optical lithography is of key importance in the fabrication of nanoscale structures, with particular relevance to the semiconductor industry, however, it is limited by diffraction. Advancements in alternative optical lithography techniques that circumvent this diffraction limit will enable applications of nanopatterning, such as 3-dimensional fabrication of nanostructures for biological applications. In this article, we review a class of optical lithographic techniques that achieve deep sub-wavelength resolution using photoswitchable molecules. We call this approach Patterning via Optical-Saturable Transformations (POST).[1]

In POST, a thin layer of photochromic molecules is used as the pattern-recording material. The principle of operation is related to nanoscale fluorescent imaging where the samples are labeled with photoswitchable fluorophores such as in stimulated emission-depletion (STED) microscopy.[2] In STED, a focused round spot first excites the fluorophores in a diffraction-limited region (Fig. 1(b)). Subsequently, a focused ring-shaped spot at a longer wavelength de-excites the molecules through stimulated emission in this region except at the center of the ring (Fig. 1(c)). Only fluorophores in the center of the ring remain in the excited state and spontaneously emit photons (Fig. 1(d)). This light-emitting region can be substantially smaller than the far-field diffraction limit. In nanopatterning, a "locking" step is necessary to fix the sub-wavelength region, and isolate it from further optical processing. The photochromic molecule used in POST exists in two isomeric states. One of the isomers may be selectively and irreversibly converted ("locked") into a 3rd state (Fig. 1(e)). An illustration of the sequence of steps in POST is shown in Figs. 1(f)–1(p).

The photochromic layer is originally in one homogeneous state as shown in Fig. 1(f). When this layer is exposed to a focused node at λ_2, it converts into the second isomeric state (shown in red) everywhere except in the near vicinity of the node. By controlling the exposure dose, the size of the unconverted region may be made arbitrarily small (Fig. 1(h)). A subsequent locking step "locks" in the pattern (Fig. 1(i)). Next, the layer is exposed uniformly to λ_1, which converts everything except the locked region back to the original state (shown in white in Fig. 1(k)). The sequence of steps may be repeated with a displacement of the sample relative to the optics, resulting in two "locked spots" whose spacing is smaller than the far-field diffraction limit (Fig. 1(p)). Therefore, any arbitrary geometry may be patterned in a "dot-matrix" fashion.

It is clear from the previous discussion that the locking step is the key difference between nanoscopy and nanoscale patterning. We have pursued two alternative paths to achieve this locking behavior. Clearly, the molecule that is used for recording will determine the specific approach. In our examples, we used a diarylethene molecule, specifically (1, 2-bis(5, 5′-dimethyl-2, 2′-bithiophen-yl) perfluorocyclopent-1-ene. Colloquially, we refer to this compound as BTE. BTE exists in two isomeric forms as illustrated in Fig. 2(a).

The closed-ring isomer has an extended conjugation of its π electron cloud, which allows the closed-ring isomer to have a lower oxidation potential than the open-ring isomer.[3]

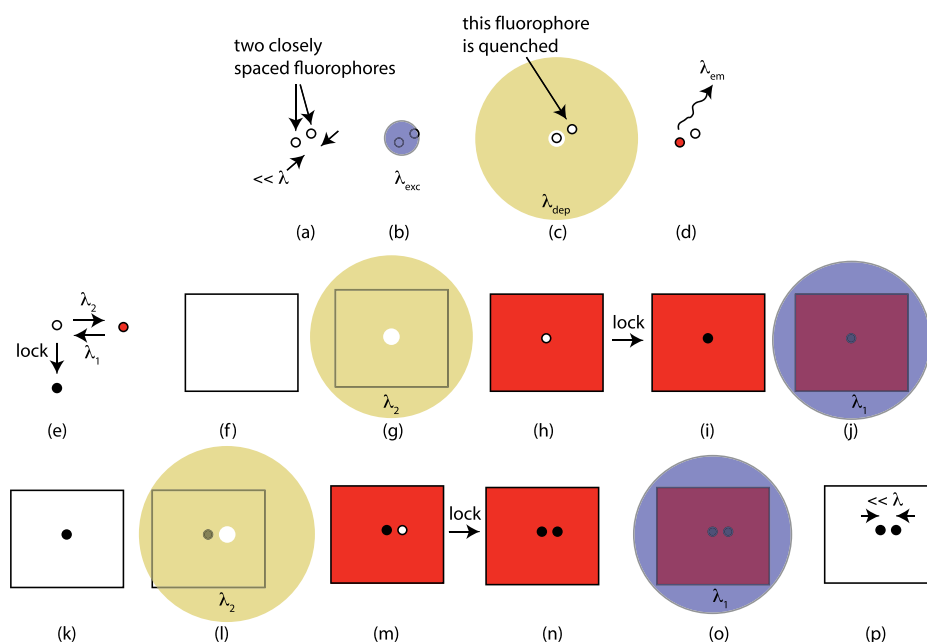a)Email: cantu@eng.utah.edu

105, 193105-1

FIG. 1. (a)–(d) Schematic of stimulated-emission-depletion microscopy. (e)–(p) Schematic of POST.

Our first approach to "locking" therefore relies on the selective oxidation of the closed-ring isomer.

The locking step is achieved by electrochemical oxidation of the closed-ring isomer into a stable cation. This product cation is preferentially soluble in a polar solvent compared to the unoxidized isomers. Therefore, it allows us to convert the locked regions into topographic nanoscale patterns after all the exposures are completed. The idea is illustrated in Fig. 2(b).

The sample is comprised of a clean silicon wafer onto which a 100 nm-thick film of Pt is evaporated. Subsequently, about 20 nm of BTE is thermally evaporated on top of the Pt.
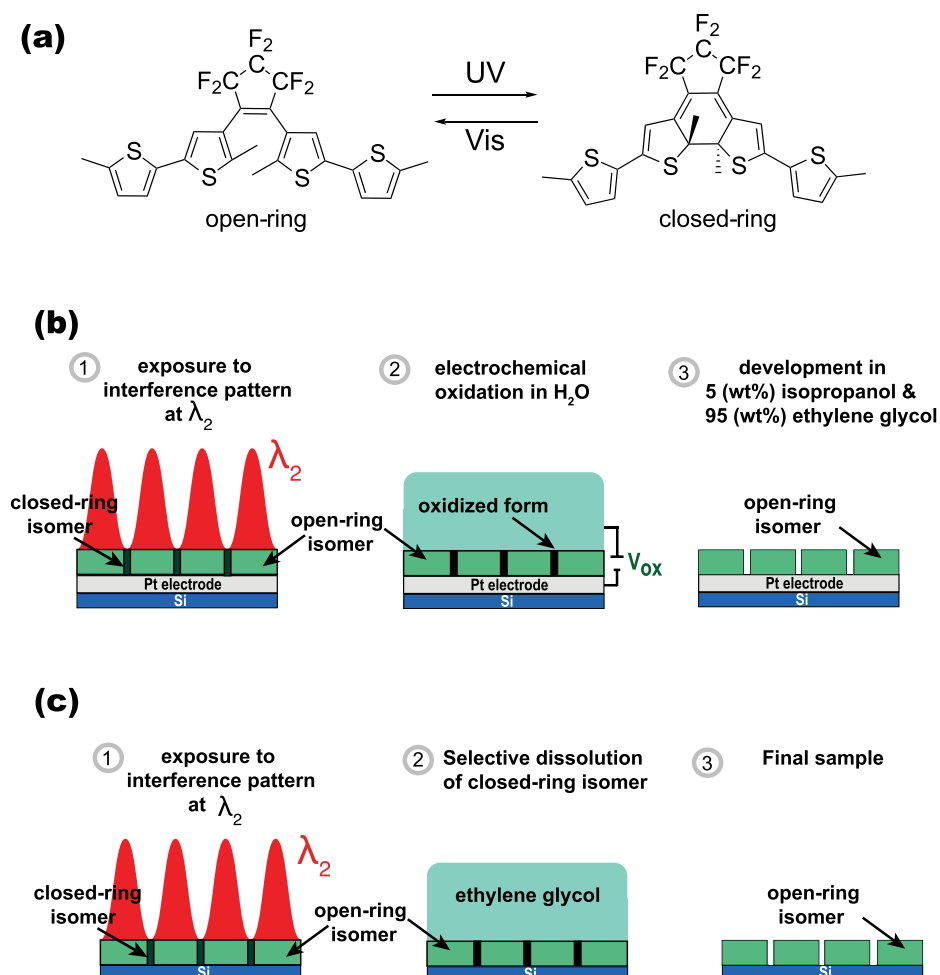

FIG. 2. (a) Schematic of photochromic molecule (BTE) used in POST. (b) Electrochemical oxidation as the locking step in POST. (c) Isomer-selective dissolution as the locking step.

Prior to use, all the BTE is converted into the closed-ring form. In step 1, the sample is exposed to a standing wave at a visible wavelength ($\lambda_2 = 633$ nm), where all the BTE is converted to the open-ring form except in very narrow lines near the vicinity of the nodes of the standing wave. For a single-exposure experiment, the sample is then placed in an electrochemical cell and oxidized at about 0.5 V. This converts only the closed-ring isomer into a cation, while the open-ring isomer is unaffected. Finally, in step 3, the sample is developed in a mixture of 95 (wt. %) ethylene glycol and 5 (wt. %) isopropanol, which dissolves away the cations. Most of the unoxidized BTE remains. This results in nanoscale grooves as illustrated. The width of these grooves is no longer determined primarily by the far-field diffraction limit (which in this case should be half the period of the exposing standing wave). The details of this experiment and related approaches have been described previously by Brimhall et al. and Cantu et al.[1,4]

An alternative approach to the locking mechanism has also been identified. The idea is based upon the selective dissolution of one of the isomers of the BTE. This has the advantage of not requiring a conductive Pt layer, which might be problematic in some devices. Also, it combines the two steps of locking and development into a single dissolution step. The idea is illustrated in Figure 2(c).

We have recently realized that two isomers of BTE have drastically different solubility rates in ethylene glycol. Hence, it allowed us to realize preliminary experimental results from this approach.[5]

We have recently developed a simple model to describe POST, which allows us to explain the observed experimental results well. The salient features of this model and related simulation analysis are summarized here.

The geometry of the problem is illustrated in Fig. 3(a). The propagation of light is from top to bottom (in the positive Z direction). A two-dimensional geometry is assumed. This is consistent with our experiments, where a 1-D standing wave is used for exposure. The chemical rate equation

for the reaction from the closed-form [C] (which is the initial form of all molecules) to the open-form [O] is given by

$$-\frac{\partial [C]}{\partial t} = [C] I \varepsilon_c \phi_{C \to O} - [O] I \varepsilon_o \phi_{O \to C}, \tag{1}$$

where [C] and [O] are the molar concentrations of the closed and open form isomers, respectively, ε is the molar absorptivity, ϕ is the quantum efficiency, and I is the intensity of the exposure. The differential form of the Beer-Lambert law gives us the following equation:

$$\frac{\partial I}{\partial z} = -\left(\varepsilon_O [O] + \varepsilon_C [C]\right) I. \tag{2}$$

From conservation of matter, we have

$$[O] + [C] = [C_0]. \tag{3}$$

$[C_0]$ is the initial concentration of the closed form (the only form present at the beginning). The boundary condition is $I(x, z = 0, t) = I_0(x)$, the incident illumination intensity and the initial condition are $[C_0](x, z, t = 0) = [C_0]$. For BTE, we can make the further assumption that $\phi_{O \to C}$ is 0, since visible photons do not have sufficient energy to initiate the ring-closing reaction. Since $\varepsilon_O \ll \varepsilon_C$, we can ignore ε_O in the system of equations as well. We can solve the resulting system of partial differential equations using standard finite-element methods as a function of space (x,z) and time (t).

A representative solution for the concentration distributions of open- and closed-ring isomers as a function of depth is illustrated in Fig. 3(a). A standing wave of period 600 nm and $\lambda_2 = 633$ nm was assumed for the incident illumination. Material parameters were all used from Andrew et al.[6] The thickness of the BTE layer was assumed to be 50 nm.

The electrochemical oxidation of BTE proceeds along two different paths as illustrated below. The closed-ring isomer oxidizes to a stable cation. The open-ring isomer oxidizes to a meta-stable state that can undergo photocyclization reaction and form the closed-ring isomer.[3] Here, we model these two reactions with four rate equations, Fig. 3(b)

$$\frac{\partial [O]^*}{\partial t} = k_1 [O] - k_1' [O]^*, \tag{4}$$

$$\frac{\partial [C]^+}{\partial t} = k_2 [C], \tag{5}$$

$$\frac{\partial [C]}{\partial t} = -k_2 [C] + k_1' [O]^*, \tag{6}$$

$$\frac{\partial [O]}{\partial t} = -k_1 [O]. \tag{7}$$

The solutions for this system of rate equations is

$$[O] = [O_0] e^{-k_1 t}, \tag{8}$$

$$[O]^* = \frac{[O_0] k_1}{k_1 - k_1'} e^{-k_1' t} \left\{ 1 - e^{-(k_1 - k_1') t} \right\}, \tag{9}$$
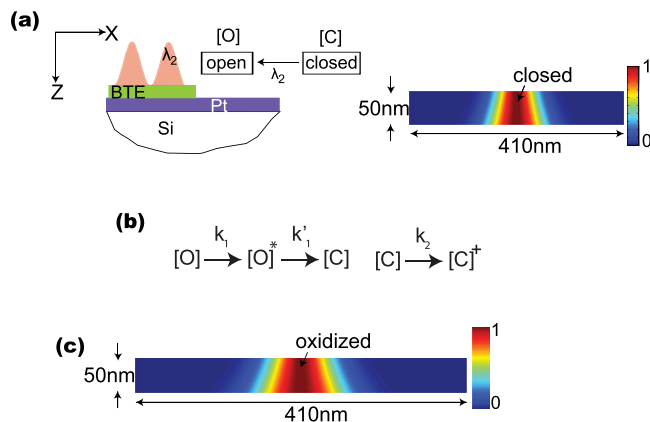

FIG. 3. (a) Model for simulating the exposure step. An example of the output of the simulation showing the relative concentrations of the two isomers within the layer. Scale bar represents normalized concentration of closed-ring isomer. (b) Electrochemical oxidation of the two isomers of BTE. (c) Normalized concentration of the oxidized-closed form of BTE. Oxidation was performed after the exposure in (a).
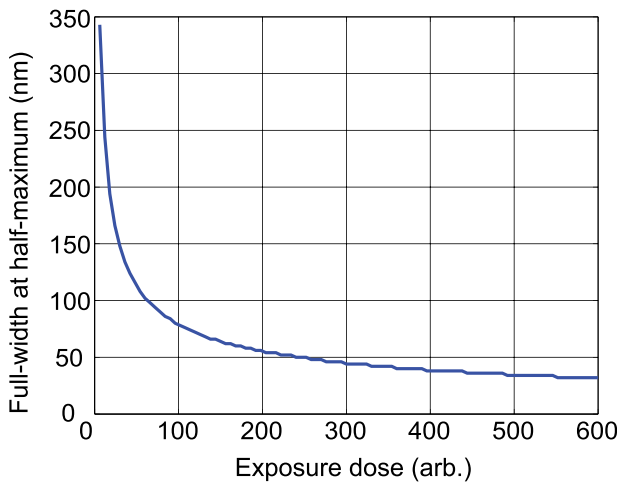
FIG. 4. Full-width at half-maximum of a developed line as a function of exposure dose. The exposure conditions were the same as in Fig. 3(a) except the period of the standing wave, which was 610 nm.

$$[C] = [C_0]e^{-k_2 t} + \frac{k_1 k_1'}{k_1 - k_1'} e^{-k_2 t}$$

$$\times \left\{ \frac{1 - e^{-(k_1' - k_2)t}}{k_1' - k_2} - \frac{1 - e^{-(k_1 - k_2)t}}{k_1 - k_2} \right\}, \quad (10)$$

$$[C]^+ = [C_0] + [O_0] - ([C] + [O] + [O]^*). \quad (11)$$

The last equation comes from the conservation of matter. Note that the subscript 0 refers to the concentration after exposure and prior to oxidation. Figure 3(c) shows an example simulation that illustrates the concentration distribution of the oxidized closed form. The rate constants need to be experimentally determined. Our previous work elucidated some of these rate constants.[1] In the simulations here, we assumed that $k_1 = 3 \times 10^{-4} min^{-1}$ and $k_2 = 1.4 \times 10^{-2} min^{-1}$. Since the rate of oxidation of the closed form is over 2 orders of magnitude higher than that of the open form, we can ignore k_1. Furthermore, if the oxidation is performed for a time that is substantially larger than $\frac{1}{k_2}$, all the closed form will be oxidized without oxidizing any of the open form. This is consistent with Fig. 3(c), where the distribution of the closed-oxidized form is almost identical to the distribution of the closed-form in Fig. 3(a).

For simplicity, we assumed that the unoxidized forms are not dissolved in the developer, while the closed-oxidized form is completely dissolved. This is a good approximation as described earlier in Brimhall et al.[1] Therefore, one would expect the final feature profile within BTE to resemble Fig. 3(c), where the red regions are removed after development. Indeed, we reported in Brimhall et al. that careful scanning-electron microscopy of the developed lines reveal a clear undercut as predicted by the simulations here.[1]

One important point to note is that the simulation model described here can be used to model POST with either locking approaches. In the case of locking using solubility differences, the oxidation simulation is not required. We can see that Figs. 3(a) and 3(c) look almost identical. This suggests that in both locking approaches, one can use only the exposure model as long as the electrochemical oxidation is performed long enough and the solubility difference between the open and closed forms is large.

We applied the model developed in Modeling and Simulation section to elucidate several key aspects of POST. First, one would expect the linewidth of the developed feature to decrease with exposure dose, since the feature is defined via the optical node. Figure 4 shows the simulation of the full-width at half-maximum (FWHM) of a developed line as a function of exposure dose to the optical standing wave. A steep decrease is seen and the FWHM continues to decrease monotonically with increasing exposure dose.

It is clear that the darkness of the optical node is critical for high contrast in POST. This idea is illustrated by simulating the effect of exposure on a BTE film by a standing wave with a perfect node (on the left) and an imperfect node (on the right) in Fig. 5. As the exposure time increases (top to bottom), for both cases, the region that remains in the closed form gets smaller. This is consistent with Fig. 4. However, for the imperfect node, noise in the node starts to convert some of closed form into the open form, which degrades the image of the patterned region. Eventually, this limits the resolution of the technique.

In this paper, we briefly reviewed the approaches that are enabling optical nanopatterning beyond the far-field diffraction limit. The basic principle is inspired by the idea of saturating an optical transition with a focal ring, which has been implemented in microscopy. However, in order to extend this principle to patterning, a "locking" mechanism is required. We described two distinct approaches to this locking mechanism. We also developed
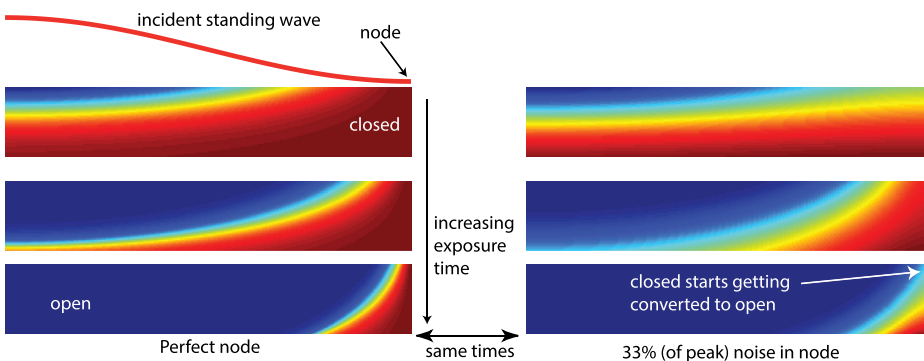

FIG. 5. Simulation of BTE isomer distribution after exposure for a standing wave with a perfect node (on the left) and for the same standing wave with a node containing noise intensity of about 33% of the peak intensity.

a simple model that simulates the steps and discussed the impact of the key parameters, particularly the quality of the node.

[1]N. Brimhall, T. L. Andrew, R. V. Manthena, and R. Menon, Phys. Rev. Lett. **107**, 205501 (2011).
[2]S. W. Hell, Science **316**, 1153 (2007).
[3]A. Peters and N. R. Branda, Chem. Commun. **8**, 954–955 (2003).
[4]P. Cantu, T. L. Andrew, R. Castagna, C. Bertarelli, and R. Menon, Appl. Phys. Lett. **100**, 183103 (2012).
[5]P. Cantu, T. L. Andrew, and R. Menon, Appl. Phys. Lett. **103**, 173112 (2013).
[6]T. L. Andrew, H. Y. Tsai, and R. Menon, Science **324**(5929), 917–921 (2009).